

# CNN-based Euler’s Elastica Inpainting with Deep Energy and Deep Image Prior

Karl Schrader\*, Tobias Alt\*, Joachim Weickert\*, Michael Ertel\*

\* Mathematical Image Analysis Group

Faculty of Mathematics and Computer Science, Campus E1.7, Saarland University, 66041 Saarbrücken, Germany

Email: {schrader, alt, weickert, ertel}@mia.uni-saarland.de

**Abstract**—Euler’s elastica constitute an appealing variational image inpainting model. It minimises an energy that involves the total variation as well as the level line curvature. These components are transparent and make it attractive for shape completion tasks. However, its gradient flow is a singular, anisotropic, and nonlinear PDE of fourth order, which is numerically challenging: It is difficult to find efficient algorithms that offer sharp edges and good rotation invariance. As a remedy, we design the first neural algorithm that simulates inpainting with Euler’s Elastica. We use the deep energy concept which employs the variational energy as neural network loss. Furthermore, we pair it with a deep image prior where the network architecture itself acts as a prior. This yields better inpaintings by steering the optimisation trajectory closer to the desired solution. Our results are qualitatively on par with state-of-the-art algorithms on elastica-based shape completion. They combine good rotation invariance with sharp edges. Moreover, we benefit from the high efficiency and effortless parallelisation within a neural framework. Our neural elastica approach only requires  $3 \times 3$  central difference stencils. It is thus much simpler than other well-performing algorithms for elastica inpainting. Last but not least, it is unsupervised as it requires no ground truth training data.

**Index Terms**—image inpainting, variational methods, CNNs, deep energy, deep image prior, Euler’s elastica

## I. INTRODUCTION

Inpainting [1]–[3] aims at reconstructing missing regions of an image in a semantically plausible way. In the last two decades, many inpainting techniques have been proposed using model-based [4] ideas as well as deep learning [5], [6]. A particularly well-researched variational model goes back to Mumford [7] and utilises Euler’s elastica [8]. It minimises an energy with a total variation and a curvature term. Both terms offer a clear interpretation for shape completion tasks and lead to a particularly transparent model.

Unfortunately, the numerical minimisation of this nonconvex energy is highly nontrivial, since its gradient flow is a singular, anisotropic nonlinear partial differential equation (PDE) of order four. It is difficult to find efficient algorithms that produce sharp edges, offer a good approximation of rotation invariance, and can inpaint large gaps. Numerous numerical ideas have been proposed to tackle this challenging task, including multigrid techniques [9], discrete gradient

methods [10], augmented Lagrangian approaches [11], operator splitting [12], and lifting concepts [13]; see [14] for an overview and additional references. To the best of our knowledge, however, no deep neural networks have been used for solving elastica inpainting. In view of the success of convolutional neural networks (CNNs) [15] in all visual computing fields as well as in numerical analysis, this is surprising. The goal of our paper is to close this gap.

**Our Contributions.** Our approach focuses on *deep energies* [16]. It uses the variational energy as loss function for training a neural network without ground truth data. For digital images, this only requires to discretise the energy. The task of its numerical minimisation via gradient descent is delegated to the neural network. In this way we benefit from its powerful optimisation algorithms and an effortless parallelisation on GPUs. It should be noted that the discretisation of the elastica energy only involves first and second order derivatives. This is far more pleasant than discretising a fourth order gradient flow. We show that  $3 \times 3$  central differences with optimised rotation invariance are sufficient for this task.

While our discrete energy is simple, it cannot penalise checkerboard-like artefacts. As a remedy, we employ a second neural concept, namely *deep image priors* [17]: This approach reparametrises an image as the output of a neural network and has a regularising effect. It efficiently prevents the introduction of unnatural artefacts into the resulting image.

Our experiments show that both neural components are essential for obtaining a good minimiser of the elastica energy. We even reach the quality of a sophisticated state-of-the-art algorithm. Our approach is efficient, offers sharp results with good rotation invariance, and can bridge large gaps.

**Related Work.** Combinations of Euler’s elastica and neural concepts are rare and restricted to areas beyond image inpainting. The use of elastica for supervised classification is investigated in [18]. There, they act as a regulariser on the level lines of a learned classifier. An elastica-based segmentation model where the minimiser is predicted by a neural network was explored in [19].

Inpainting models that rely on deep learning can produce visually realistic images; see e.g. [5], [6]. However, they require tremendous amounts of training data, and uncovering the

This work has received funding from the European Research Council (ERC) under the European Union’s Horizon 2020 research and innovation program (grant agreement no. 741215, ERC Advanced Grant INCOVID).

learned model is infeasible due to the large number of trainable parameters. The concept of deep energies [16] follows a different philosophy by proposing to use classical variational energy models as loss functions for neural networks. Deep energy models require no ground truth training data, and the mathematical model is fully defined by the energy.

Deep image priors [17] have shown how the architecture of a neural network can act as a regularising prior on its output [20]. They preserve natural visual objects while attenuating noise. Therefore, their optimisation trajectories pass close by the desired solution in tasks such as noise or artefact removal. Many works build upon this concept and propose different strategies for stopping the iteration as close as possible to the desired solution; see e.g. [21] and the references therein.

**Organisation of the Paper.** In Section II, we briefly review Euler’s elastica model for inpainting. Afterwards, in Section III, we introduce our neural algorithm. We evaluate it in Section IV and present our conclusions in Section V.

## II. REVIEW: ELASTICA INPAINTING

Let  $f : \Omega \rightarrow \mathbb{R}$  denote a continuous greyscale image that is only known on an *inpainting mask*  $K$ , a subset of the rectangular image domain  $\Omega$ . Inpainting aims at reconstructing  $f$  in the *inpainting domain*  $\Omega \setminus K$ . Euler’s elastica obtain such a reconstruction  $u$  as a minimiser of the energy

$$E(u) = \int_{\Omega \setminus K} |\nabla u| \left( b + (1 - b) \kappa^2 \right) dx dy. \quad (1)$$

On the inpainting mask  $K$ , we enforce  $u = f$ . The energy (1) combines the total variation (TV) [22] penaliser  $|\nabla u|$  with the level line curvature  $\kappa = \nabla^\top \left( \frac{\nabla u}{|\nabla u|} \right)$ , where  $\nabla = (\partial_x, \partial_y)^\top$  is the nabla operator, and  $|\cdot|$  denotes the Euclidean norm. The balance between the two components is steered by a parameter  $b \in [0, 1]$ . It can produce results from pure contour length minimisation (for  $b = 1$ ) to pure curvature minimisation ( $b = 0$ ). Both components are highly desirable and psychophysically relevant for shape completion [23].

Although the elastica energy (1) is transparent, it involves many inherent problems:  $|\nabla u|$  is nondifferentiable in  $\mathbf{0}$ , and dividing by it within the curvature term may create singularities. Moreover, since  $|\nabla u| \kappa$  is the second derivative of  $u$  in level line direction, the elastica energy is highly anisotropic. It is also nonconvex and may thus have numerous local minimisers. Any minimiser is a steady state of the gradient flow PDE of the energy. Since the energy (1) is nonquadratic, its gradient flow is nonlinear. Moreover, (1) involves derivatives up to order two. This creates a gradient flow of order four; see [24] for an explicit formula. Fourth order PDEs are numerically much harder to solve than the widespread second order ones. Other challenges such as nondifferentiability, singular behaviour, and anisotropy are inherited.

As already mentioned, these problems directly lead to numerous numerical challenges. They have inspired many

researchers to develop highly sophisticated algorithms for elastica inpainting. We show that the concepts of deep energies and deep priors help us to make these problems more manageable and lead to a simple and well-performing algorithm.

## III. SOLVING ELASTICA WITH DEEP LEARNING

Our paper follows the *discretise then optimise* paradigm. Discretising the energy rather than its fourth order gradient flow allows us to restrict ourselves to derivatives up to order two. Moreover, we know that the resulting algorithm minimises a discrete energy, which we can use to monitor its success. Most importantly, however, we can exploit the capabilities of neural networks to minimise difficult nonconvex energies in an efficient way.

### A. Discretising the Elastica Energy

The components of the energy (1) can be spelled out as

$$|\nabla u| \approx \sqrt{u_x^2 + u_y^2 + \varepsilon^2}, \quad (2)$$

$$\kappa \approx \frac{u_y^2 u_{xx} - 2u_x u_y u_{xy} + u_x^2 u_{yy}}{(u_x^2 + u_y^2 + \varepsilon^2)^{\frac{3}{2}}}, \quad (3)$$

where subscripts denote partial derivatives. Regularising  $|\nabla u|$  with  $\varepsilon > 0$  avoids nondifferentiability and division by zero.

We obtain discrete images  $u, f$  by sampling the continuous functions  $u, f$  on a uniform grid with distance  $h$ . We represent images as vectors by stacking the grey values into a column vector. Moreover, we consider a discrete binary inpainting mask  $c$  as an indicator image of the set  $K$ . A value of 1 marks known data, and 0 indicates the inpainting domain.

Finite difference discretisations of derivatives are always a compromise between many criteria: Ideally they are simple, offer good rotation invariance, do not introduce artificial blur, and have a high approximation quality for all frequencies. In practice, improving the performance w.r.t. one criterion often comes at the expense of another. Our discretisation prioritises *simplicity* and good *rotation invariance*, since both are frequent weaknesses of existing elastica algorithms. We shall also see that it does not create blurry edges. Its main drawback are checkerboard artefacts in the highest grid frequency. We will cure them with a deep image prior.

For *simplicity*, we approximate all derivatives by finite differences on a  $3 \times 3$  stencil, which allows consistency order two. To guarantee that they all fit together, we obtain them jointly from the coefficients of a weighted least squares regression polynomial of order two. We achieve good *rotation invariance* with the tensor product of the binomial weights  $[\frac{1}{4}, \frac{1}{2}, \frac{1}{4}]$  in  $x$ - and  $y$ -direction, which approximates a rotationally invariant 2-D Gaussian. This yields

$$\partial_x \approx \frac{1}{8h} \begin{bmatrix} -1 & 0 & 1 \\ -2 & 0 & 2 \\ -1 & 0 & 1 \end{bmatrix}, \quad \partial_{xx} \approx \frac{1}{4h^2} \begin{bmatrix} 1 & -2 & 1 \\ 2 & -4 & 2 \\ 1 & -2 & 1 \end{bmatrix} \quad (4)$$

and corresponding stencils in  $y$ -direction. Note that our approximations for  $\partial_x$  and  $\partial_y$  coincide with Sobel operators,

which are well-known for their rotation invariance. For the mixed derivative we obtain (with  $y$ -axis oriented upwards)

$$\partial_{xy} \approx \frac{1}{4h^2} \begin{bmatrix} -1 & 0 & 1 \\ 0 & 0 & 0 \\ 1 & 0 & -1 \end{bmatrix}. \quad (5)$$

With these stencils and by replacing the integral by a summation over all pixels  $i$  in the inpainting domain (i.e. in locations  $i$  with  $c_i = 0$ ), we arrive at our discrete counterpart of (1):

$$E(\mathbf{u}) = \sum_i (1 - c_i) |\nabla \mathbf{u}|_i \left( b + (1 - b) \kappa_i^2 \right). \quad (6)$$

### B. Minimisation via Deep Energies

To minimise this energy with advanced variants of gradient descent, we use it as a loss function in a neural network. Golts et al. [16] call this a *deep energy*. Modern deep learning frameworks allow us to implement the discrete energy  $E(\mathbf{u})$  and use backpropagation [25] to evaluate  $\nabla_{\mathbf{u}} E(\mathbf{u})$ . With this we can perform gradient descent:

$$\mathbf{u}^{k+1} = \mathbf{u}^k - \tau \nabla_{\mathbf{u}^k} E(\mathbf{u}^k), \quad (7)$$

where  $\tau$  denotes the step size and superscripts the iteration level. For Euler’s elastica, this frees us from the need to find a good discretisation of a fourth-order PDE. Instead, only the energy which contains derivatives up to second order must be discretised. Its gradient is efficiently computed by the network by exploiting the parallelism of GPUs. Note that so far, our network is used as a pure optimisation tool. It has no trainable weights apart from the iteratively inpainted image  $\mathbf{u}^k$ .

### C. Regularisation with a Deep Image Prior

By design, our finite difference stencils (4)–(5) are simple and offer good rotation invariance. However, it is easy to see that the discrete elastica energy does not penalise oscillations with the highest grid frequency, where both Sobel operators return zero. As a result, checkerboard artefacts can appear. We avoid them with the regularising properties of a deep image prior [17], [20]: It has been shown that typical neural networks converge rapidly towards natural images while attempting to avoid unnatural artefacts. As a consequence, our resulting model first recovers an image that fulfils the desired elastica properties, and may introduce undesirable artefacts afterwards. Thus, stopping the minimisation at the right time is crucial.

We impose a deep prior on  $\mathbf{u}$  by replacing it by the output of a network  $\mathbf{u} = \mathcal{N}(\mathbf{c}, \mathbf{f}, \boldsymbol{\theta})$  with mask  $\mathbf{c}$  and known grey values  $\mathbf{f}$  as inputs, and parametrised by weights  $\boldsymbol{\theta}$ . Instead of searching for the minimiser  $\mathbf{u}$  directly, we are now solving for the weights  $\boldsymbol{\theta}$  which minimise  $E(\mathcal{N}(\mathbf{c}, \mathbf{f}, \boldsymbol{\theta}))$ . Gradient descent gives

$$\boldsymbol{\theta}^{k+1} = \boldsymbol{\theta}^k - \tau \nabla_{\boldsymbol{\theta}^k} E(\mathcal{N}(\mathbf{c}, \mathbf{f}, \boldsymbol{\theta}^k)). \quad (8)$$

Note the close connection to the explicit scheme (7), as the gradient w.r.t. the weights is computed via the chain rule. With  $\mathbf{u}^k := \mathcal{N}(\mathbf{c}, \mathbf{f}, \boldsymbol{\theta}^k)$  and the Jacobian  $\nabla_{\boldsymbol{\theta}^k} \mathbf{u}^k$ , this reads

$$\nabla_{\boldsymbol{\theta}^k} E(\mathbf{u}^k) = (\nabla_{\boldsymbol{\theta}^k} \mathbf{u}^k) \nabla_{\mathbf{u}^k} E(\mathbf{u}^k). \quad (9)$$

The gradient  $\nabla_{\mathbf{u}^k} E(\mathbf{u}^k)$  is calculated first before being distributed onto the contributing weights  $\boldsymbol{\theta}^k$ .

Our experiments will demonstrate that this deep prior regularisation efficiently attenuates checkerboard artefacts. Moreover, by avoiding irrelevant local minima, it brings us closer to the desired solution after a reasonable number of iterations.

### D. Our Inpainting Network Architecture

In Figure 1 we outline the full pipeline of our neural algorithm for elastica inpainting. As the energy is only considered within the inpainting domain, we remask the network output  $\mathbf{u}$  with the known data  $\mathbf{f}$ . The final reconstruction is passed to the deep energy loss function which evaluates its quality.

Our architecture consists of a small gated U-net [6], [26]. Ulyanov et al. [17] found that variants of U-nets perform well as deep priors for tasks like inpainting or artefact removal. Furthermore, gated U-nets were used successfully for free-form inpainting as in our setting [6], and we confirm their suitability as deep priors in our experiments.

The defining feature of U-nets is their shape: The left part consists of a sequence of convolutions and downsampling operations, resulting in features on different scales. In a similar way, the right side repeatedly convolves and upsamples the features, and it concatenates them with features of the same scale from the downsampling pass. The gated U-net enhances the architecture by jointly evolving features and masks in each gated convolutional layer; see [6] for a detailed explanation.

## IV. EXPERIMENTS

In this section we first present an ablation study which demonstrates that both neural components of our approach are essential. Afterwards we evaluate its performance for inpainting of natural images and shape completion tasks.

### A. Experimental Setup

We prefer standard U-nets for fast inpaintings of natural images, and gated ones for shape completion with highest quality. Depending on the size of the image, three or four scales with two convolutional layers each are used. We start with up to 28 channels at the finest resolution and double them with each downsampling. Following [6], dilated convolutions on the coarsest scale of the gated U-nets are included. The inpainting region of the masked image is initialised with random uniform noise in the same range  $[0, 1]$  as the image.

The network is trained with the Adam optimiser [27]. We start with a learning rate of  $\tau = 0.001$  for natural images and  $\tau = 0.00005$  for shape completion and decrease it in later epochs. The parameter  $b$  is chosen as to minimise the mean absolute error (MAE) w.r.t. the ground truth. We use the MAE since it better reflects our visual impression than the mean squared error (MSE), while remaining mathematically more transparent than pure perceptual measures.

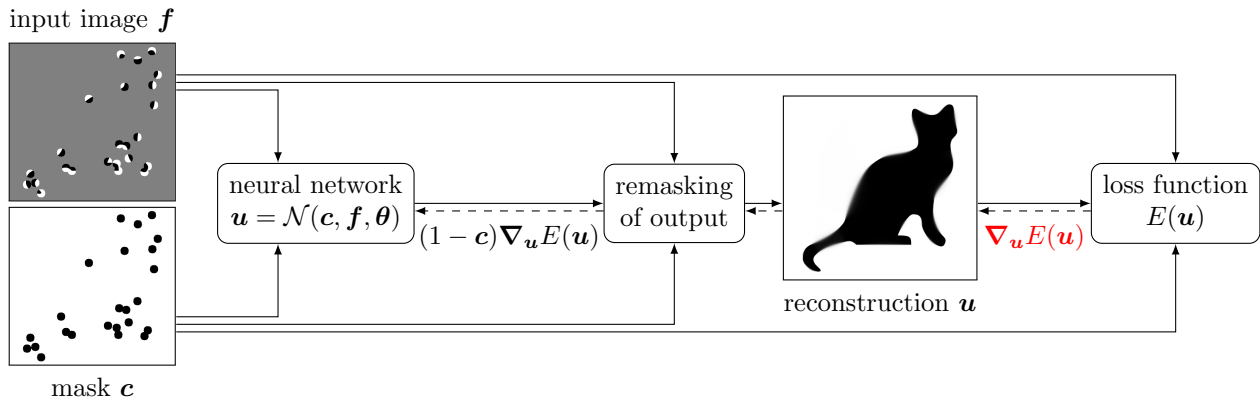


Fig. 1. The full network architecture. The flow of gradients during backpropagation is depicted with dashed lines. Notice that  $\nabla_u E(u)$  is still computed as part of the backpropagation, which shows the close connection to gradient descent.

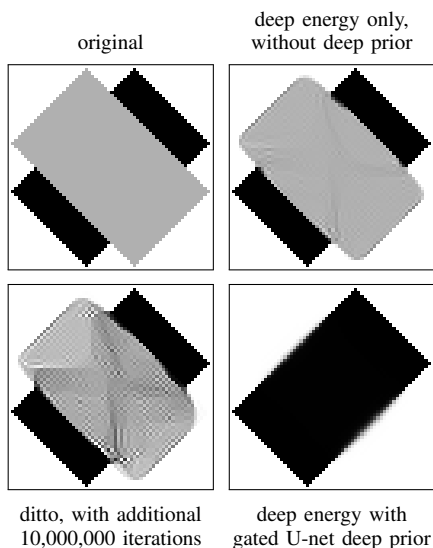


Fig. 2. Comparison of results with and without deep prior ( $b = 0.001$ ,  $\varepsilon = 0.0001$ , and 60,000 iterations). For simplicity, the inpainting region is initialised with the average gray value. The learning rate starts at  $\tau = 0.00004$  and is halved every 20,000 iterations. The optimisation producing the third image ran for an additional 10,000,000 iterations at the final learning rate.

### B. Ablation Study

The ablation study in Figure 2 shows that the deep energy alone is insufficient for obtaining the desired inpainting result, regardless of the number of iterations. Incorporating the deep image prior is essential. It helps to escape from bad local minima: From the third to the fourth image, the discrete energy drops from 2.22 to the remarkably low value of 0.08.

### C. Inpainting of Natural Images

Figure 3 shows how our inpainting algorithm performs on natural images. After a few thousand iterations, it produces the desired result that minimises the MAE. Additional iterations still reduce the energy, but deteriorate the MAE and the visual impression; see Figure 4. The checkerboard-like artefacts in the steady state confirm the previously discussed limitations of our discrete energy. Thus, it is helpful to stop earlier and

benefit from the regularising qualities of the deep image prior. Stopping earlier also allows us to obtain our results faster. With an Nvidia GTX 1080 GPU, it takes 49 s for the 6,000 iterations needed for the  $256 \times 256$  image *trui*. Finding an automatic stopping criterion is part of our future research.

Speed comparisons to other works remain difficult as they often do not disclose their runtimes, do not make use of the GPU, or cannot produce comparable quality. A rough comparison can be made to the augmented Lagrangian approach of Tai et al. [11]. For an  $300 \times 235$  image and a fairly dense random mask with 60 % known pixels, their inpainting takes 78 s on an Intel Core 2 Duo P8600 @ 2.4 GHz CPU. Yashtini and Kang [12] propose an ADMM method and report 854 s for inpainting a  $220 \times 340$  colour image with a random mask with 20 % density on a 2.5 GHz Intel Core i5 CPU. These numbers indicate that our algorithm offers a competitive speed.

### D. Shape Completion

Shape completion allows us to demonstrate that our discretisation produces sharp and rotation invariant results. In Figure 5, we show that completion of straight edges, curves, and combinations thereof are handled adequately. Most noticeably, very large gaps with almost 200 pixels between the mask regions can be closed. In Figure 6 we compare to the state-of-the-art results obtained with the sophisticated lifting approach of Chambolle and Pock [13]. While our neural algorithm is simpler, it produces inpaintings of comparable visual quality.

## V. CONCLUSIONS

We have proposed the first neural algorithm for Euler's elastica inpainting. Research on numerical methods for this attractive but difficult inpainting model has been pursued for more than two decades and produced highly sophisticated techniques. It is thus surprising that our very simple approach is qualitatively competitive to a leading elastica algorithm for shape completion. This speaks for the quality of its parts and the fruitful synergy between model-based concepts and deep neural networks. Our finite difference approximations for the first and second order derivatives of the elastica energy offer

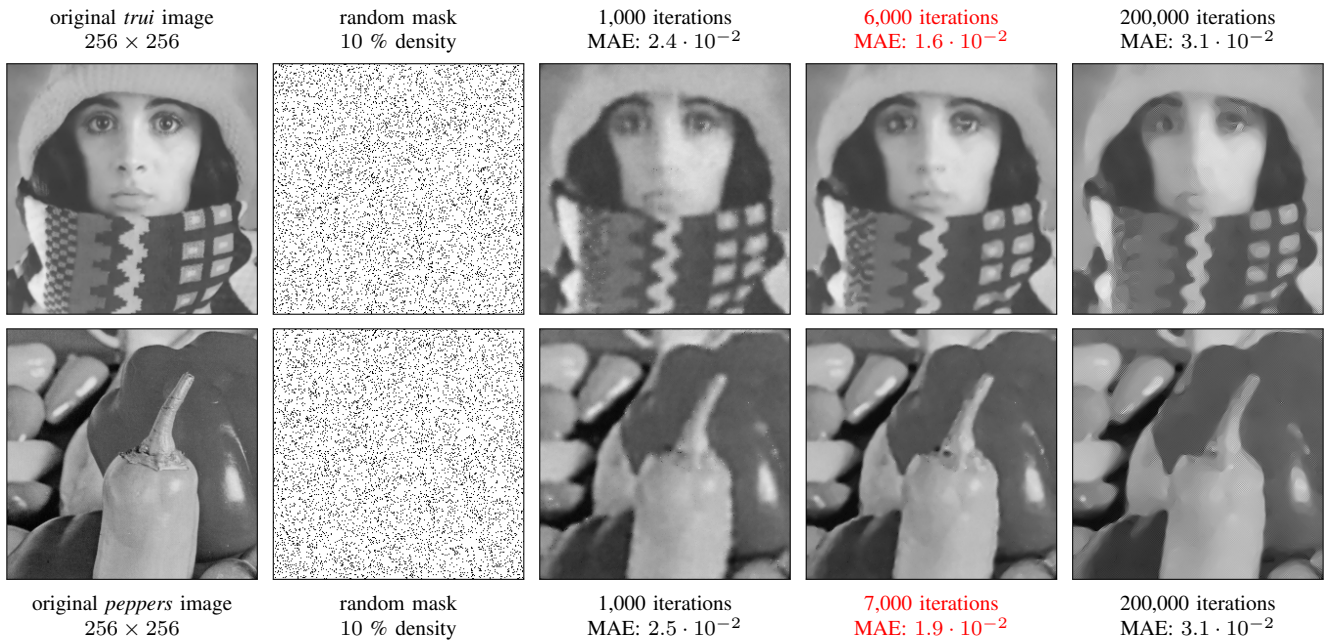


Fig. 3. Inpainting results for *trui* and *peppers* ( $b = 0.175$ ,  $\varepsilon = 0.005$ ,  $\tau = 0.001$ ). After 6000–7000 iterations, a good reconstruction with low mean average error (MAE) is obtained. Additional iterations produce checkerboard artefacts (digital zoom recommended).

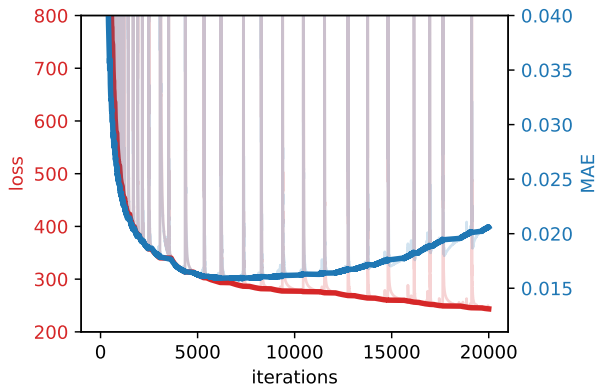


Fig. 4. Energy and reconstruction error over time corresponding to *trui* in Figure 3. Spikes were filtered from the bold lines to make the general trends more recognisable. They are caused by brief, very large gradients generated by the curvature term which cause the network to erroneously change the global brightness, but are quickly recovered from.

good rotation invariance and sharpness. Energy minimisation is accomplished automatically by a neural network that frees us from the burden of discretising the numerically challenging fourth order Euler–Lagrange PDE. Moreover, the regularising properties of a deep image prior avoid high-frequent artefacts that the discrete energy cannot penalise. In contrast to purely data-driven neural approaches, our hybrid algorithm requires neither ground truth inpaintings nor training data.

Our findings suggests that solvers which combine explicit model assumptions with deep energies and deep priors are serious competitors in challenging numerical problems. They are particularly useful when purely model-based algorithms are difficult to design, too slow, or too complex to be analysed. Since these challenges are fairly common in advanced

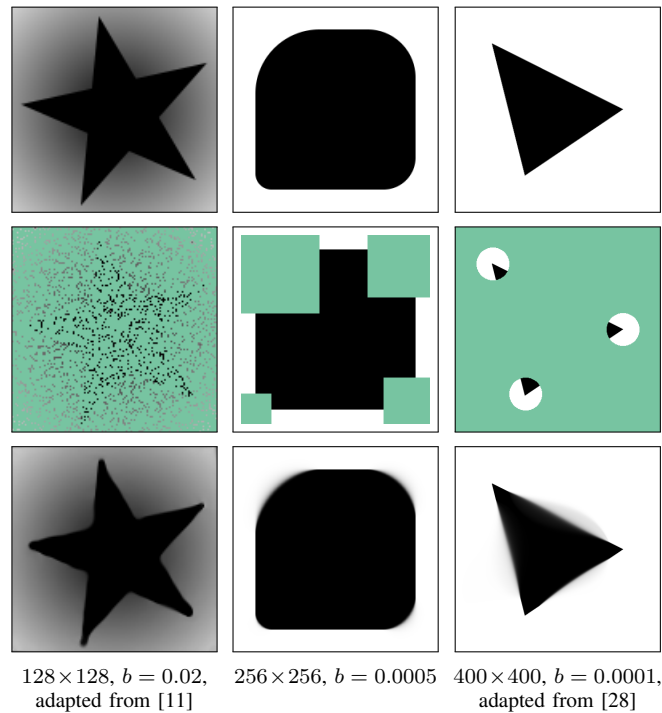


Fig. 5. Neural inpainting results on shape completion tasks ( $\varepsilon = 0.0001$ ). From top to bottom: Original, inpainting domain (in green), inpainting result.

scientific computing applications, we expect that the impact of such neuroexplicit algorithms will grow.

## REFERENCES

- [1] S. Masnou and J.-M. Morel, “Level lines based disocclusion,” in *Proc. 1998 IEEE International Conference on Image Processing*, vol. 3. Chicago, IL: IEEE Computer Society Press, Oct. 1998, pp. 259–263.



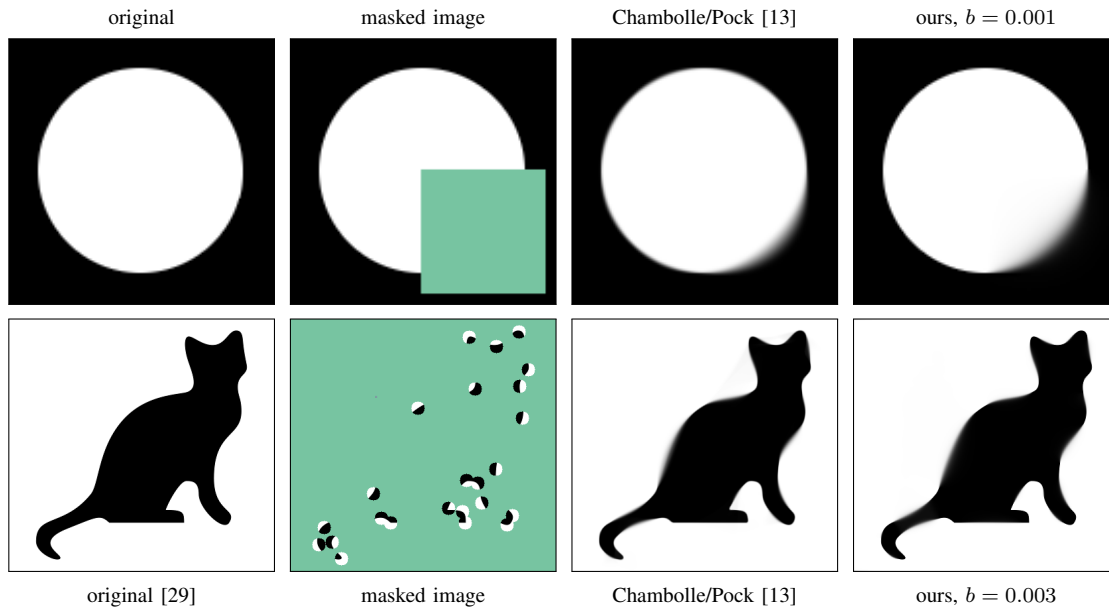


Fig. 6. Comparison to the TSC shape completion results of Chambolle and Pock [13], kindly provided by the authors ( $\epsilon = 0.0001$ ). Following their experiment, we also initialised the inpainting region of the masked image with grey value 0.5.

- [2] A. A. Efros and T. Leung, "Texture synthesis by non-parametric sampling," in *Proc. Seventh International Conference on Computer Vision*, vol. 2. Kerkyra, Greece: IEEE Computer Society Press, Sep. 1999, pp. 1033–1038.
- [3] M. Bertalmío, G. Sapiro, V. Caselles, and C. Ballester, "Image inpainting," in *Proc. SIGGRAPH 2000*, New Orleans, Jul. 2000, pp. 417–424.
- [4] C. Guillemot and O. Le Meur, "Image inpainting: Overview and recent advances," *IEEE Signal Processing Magazine*, vol. 31, no. 1, pp. 127–144, 2014.
- [5] D. Pathak, P. Krähenbühl, J. Donahue, T. Darrell, and A. A. Efros, "Context encoders: Feature learning by inpainting," in *Proc. 2016 IEEE Conference on Computer Vision and Pattern Recognition*. Las Vegas, NV: IEEE Computer Society Press, Jun. 2016, pp. 2536–2544.
- [6] J. Yu, Z. Lin, J. Yang, X. Shen, X. Lu, and T. Huang, "Free-form image inpainting with gated convolution," in *Proc. 2019 International Conference on Computer Vision (ICCV)*, vol. 1. Seoul, Korea: IEEE Computer Society Press, Oct. 2019, pp. 4470–4479.
- [7] D. Mumford, "Elastica and computer vision," in *Algebraic Geometry and its Applications*, C. L. Bajaj, Ed. New York: Springer, 1994, vol. 5681, ch. 31, pp. 491–506.
- [8] L. Euler, *Methodus inveniendi lineas curvas maximi minimive proprietate gaudentes, sive solutio problematis isoperimetrici latissimo sensu accepti*. Lausanne: Marc-Michel Bousquet et Cie., 1744.
- [9] C. Brito-Loeza and K. Chen, "Fast numerical algorithms for Euler's elastica inpainting model," *International Journal of Modern Mathematics*, vol. 5, no. 2, pp. 157–182, 2010.
- [10] T. Ringholm, J. Lazić, and C.-B. Schönlieb, "Variational image regularization with Euler's elastica using a discrete gradient scheme," *SIAM Journal on Imaging Sciences*, vol. 11, no. 4, pp. 2665–2691, 2018.
- [11] X. Tai, J. Hahn, and G. Chung, "A fast algorithm for Euler's elastica model using augmented Lagrangian method," *SIAM Journal on Imaging Sciences*, vol. 4, no. 1, pp. 313–344, Mar. 2011.
- [12] M. Yashtini and S. H. Kang, "A fast relaxed normal two split method and an effective weighted TV approach for Euler's elastica image inpainting," *SIAM Journal on Imaging Sciences*, vol. 9, no. 4, pp. 1552–1581, 2016.
- [13] A. Chambolle and T. Pock, "Total roto-translational variation," *Numerische Mathematik*, vol. 142, pp. 611–666, Mar. 2019.
- [14] S. H. Kang, X.-C. Tai, and W. Zhu, "Survey of fast algorithms for Euler's elastica-based image segmentation," in *Processing, Analyzing and Learning of Images, Shapes, and Forms: Part 2*, ser. Handbook of Numerical Analysis, R. Kimmel and X.-C. Tai, Eds. Amsterdam: Elsevier, 2019, vol. 20, ch. 13, pp. 533–552.
- [15] I. J. Goodfellow, Y. Bengio, and A. Courville, *Deep Learning*. Cambridge, MA: MIT Press, 2016.
- [16] A. Golts, D. Freedman, and M. Elad, "Deep energy: Task driven training of deep neural networks," *IEEE Journal of Selected Topics in Signal Processing*, vol. 15, no. 2, pp. 324–338, Feb. 2021.
- [17] D. Ulyanov, A. Vedaldi, and V. Lempitsky, "Deep image prior," in *Proc. 2018 IEEE Conference on Computer Vision and Pattern Recognition*. Salt Lake City, UT: IEEE Computer Society Press, Jun. 2018, pp. 9446–9454.
- [18] T. Lin, H. Xue, L. Wang, B. Huang, and H. Zha, "Supervised learning via Euler's elastica models," *Journal of Machine Learning Research*, vol. 16, no. 1, pp. 1532–4435, Jan. 2015.
- [19] X. Chen, X. Luo, Y. Zaho, S. Zhang, G. Wang, and Y. Zheng, "Learning Euler's elastica model for medical image segmentation," arXiv:2011.00526 [eess.IV], Nov. 2020.
- [20] S. Dittmer, T. Kluth, P. Maass, and D. Otero Bague, "Regularization by architecture: A deep prior approach for inverse problems," *Journal of Mathematical Imaging and Vision*, vol. 62, no. 3, pp. 456–470, 2020.
- [21] H. Wang, T. Li, Z. Zhuang, T. Chen, H. Liang, and J. Sun, "Early stopping for deep image prior," arXiv:2112.06074 [cs.CV], Dec. 2021.
- [22] L. I. Rudin, S. Osher, and E. Fatemi, "Nonlinear total variation based noise removal algorithms," *Physica D*, vol. 60, pp. 259–268, 1992.
- [23] G. Kanizsa, *Organization in Vision: Essays on Gestalt Perception*. New York: Praeger, 1979.
- [24] J. Shen, S. H. Kang, and T. F. Chan, "Euler's elastica and curvature-based inpainting," *SIAM Journal on Applied Mathematics*, vol. 63, no. 2, pp. 564–592, 2002.
- [25] D. E. Rumelhart, G. E. Hinton, and R. J. Williams, "Learning representations by back-propagating errors," *Nature*, vol. 323, no. 9, pp. 533–536, Oct. 1986.
- [26] O. Ronneberger, P. Fischer, and T. Brox, "U-net: Convolutional networks for biomedical image segmentation," in *Medical Image Computing and Computer-Assisted Intervention – MICCAI 2015*, ser. Lecture Notes in Computer Science, N. Navab, J. Hornegger, W. Wells, and A. Frangi, Eds. Cham: Springer, 2015, vol. 9351, pp. 234–241.
- [27] D. P. Kingma and J. Ba, "Adam: A method for stochastic optimization," in *Proc. 3rd International Conference on Learning Representations*, San Diego, CA, May 2015.
- [28] C. Schmalz, P. Peter, M. Mainberger, F. Ebel, J. Weickert, and A. Bruhn, "Understanding, optimising, and extending data compression with anisotropic diffusion," *International Journal of Computer Vision*, vol. 108, no. 3, pp. 222–240, Jul. 2014.
- [29] J. Weickert, "Mathematische Bildverarbeitung mit Ideen aus der Natur," *Mitteilungen der DMV*, vol. 20, pp. 80–92, 2012.